

Rapid cerebrovascular reactivity mapping: Enabling vascular reactivity information to be routinely acquired



Nicholas P. Blockley^{a,*}, James W. Harkin^b, Daniel P. Bulte^c

^a FMRIB Centre, Nuffield Department of Clinical Neurosciences, University of Oxford, Oxford, UK

^b Department of Physics, University of Oxford, Oxford, UK

^c Institute of Biomedical Engineering, Engineering Science, University of Oxford, Oxford, UK

ARTICLE INFO

Keywords:

Cerebrovascular reactivity
Magnetic Resonance Imaging
Hypercapnia challenge
BOLD

ABSTRACT

Cerebrovascular reactivity mapping (CVR), using magnetic resonance imaging (MRI) and carbon dioxide as a stimulus, provides useful information on how cerebral blood vessels react under stress. This information has proven to be useful in the study of vascular disorders, dementia and healthy ageing. However, clinical adoption of this form of CVR mapping has been hindered by relatively long scan durations of 7–12 min. By replacing the conventional block presentation of carbon dioxide enriched air with a sinusoidally modulated stimulus, the aim of this study was to investigate whether more clinically acceptable scan durations are possible. Firstly, the conventional block protocol was compared with a sinusoidal protocol of the same duration of 7 min. Estimates of the magnitude of the CVR signal (CVR magnitude) were found to be in good agreement between the stimulus protocols, but estimates of the relative timing of the CVR response (CVR phase) were not. Secondly, data from the sinusoidal protocol was reanalysed using decreasing amounts of data in the range 1–6 min. The CVR magnitude was found to tolerate this reduction in scan duration better than CVR phase. However, these analyses indicate that scan durations in the range of 3–5 min produce robust data.

1. Introduction

Whilst there are many clinical techniques to investigate cerebral physiology at rest, methods to examine the brain during dynamic changes in demand are few in number. Resting perfusion measurement techniques using Computed Tomography (CT) or Magnetic Resonance Imaging (MRI) are able to confirm that the tissue is well supplied at rest, but they do not provide information on how the vasculature will react during increases in demand. By introducing a physiological challenge this aspect of cerebrovascular health can be revealed. There are two main vasoactive challenges that can be used to provide a stress test of the cerebral vasculature: acetazolamide and carbon dioxide. Acetazolamide provides a large physiological challenge by maximally dilating cerebral arterioles. However, its effects are relatively long lasting (~30 min) and it therefore has the potential to interfere with the accuracy of other diagnostic measurements made in the same session. In contrast, carbon dioxide may have a weaker vasodilatory effect, but it is rapidly cleared by the lungs enabling multiple short repeated challenges to be performed without interfering with subsequent measurements. When combined with an imaging modality this carbon dioxide stimulus, often termed a

hypercapnia challenge, enables cerebrovascular reactivity (CVR) to be mapped at the tissue level. The most common imaging modality for this purpose is MRI. Measurements have been performed using both Arterial Spin Labelling (ASL) (Mandell et al., 2008) and Blood Oxygenation Level Dependent (BOLD) (Rostrup et al., 1994) weighted techniques, each with their own advantages and disadvantages. BOLD weighted imaging offers higher spatial and temporal resolution and a higher signal to noise ratio (SNR) than ASL, whereas ASL provides quantitative measurements of perfusion change and BOLD does not. In practice, BOLD weighted measurements are more commonly used due to their higher sensitivity, more widespread availability and ease of analysis.

The information provided by CVR measurements has proven useful in a range of research applications, but has yet to cross over into clinical practice. CVR mapping has perhaps made the biggest impact in the study of vascular disorders of the brain. In patients with unilateral carotid stenosis it has been used to show that CVR is reduced in both the affected and unaffected hemisphere (Sam et al., 2014). In Moyamoya patients, who share similar pathological narrowing of cerebral vessels, BOLD based CVR has been shown to give comparable results with ASL based CVR (Mandell et al., 2008). CVR measurements have also been acquired

* Corresponding author. FMRIB Centre, Nuffield Department of Clinical Neurosciences, University of Oxford, John Radcliffe Hospital, Headington, Oxford, OX3 9DU, UK.
E-mail address: nicholas.blockley@ndcn.ox.ac.uk (N.P. Blockley).

in difficult patient populations such as in subarachnoid haemorrhage (da Costa et al., 2013) or in rare conditions such as MELAS (Rodan et al., 2015) where in both cases only limited biomarkers are available. CVR has also shown promise as a biomarker in dementia and healthy ageing research. In Alzheimer's disease CVR has been shown to be altered in patients with different variants of the APOE gene (Suri et al., 2015). CVR has also been used to investigate the effect of healthy ageing on brain haemodynamics (Gauthier et al., 2013).

However, the clinical adoption of hypercapnia based CVR mapping has so far been hindered by two main challenges: (i) relatively long scan times and (ii) long patient preparation times. Clinical MRI examinations are typically split into discrete diagnostic measurements of approximately 5 min in duration. However, currently CVR examinations are between 7 and 12 min in duration, meaning that compromises in diagnostic protocols must be made to accommodate such measurements. Preparation of patients adds an additional time penalty that is dependent on the means of gas administration and/or gas sampling. However, in this study we concentrate on the question of reducing the duration of the CVR examination.

Typically, hypercapnic gas challenges are presented in blocks interleaved with a baseline air breathing condition. One popular gas protocol used by researchers in Toronto involves the use of two hypercapnic blocks of differing duration; an initial short block followed by a second much longer block (Spano et al., 2012). This protocol has also been used to derive information about the relative timing of the CVR response using Transfer Function Analysis (TFA) (Duffin et al., 2015) or by fitting a temporal model of the vascular response (Poublanc et al., 2015). This timing information has been suggested to be reflective of regional variations in blood transit time (Blockley et al., 2010) or variations in vascular response time i.e. the rate at which the CVR response develops (Duffin et al., 2015). Overall scan time can be reduced by shortening the duration of hypercapnia blocks. However, as the block duration is reduced, vascular response delays may become an increasingly large fraction of the block duration, particularly in disease (Poublanc et al., 2013). Since this delay is not typically accounted for in the analysis of such data, this may cause CVR measurements to be underestimated. Alternatively, in the limit of short blocks a sinusoidally varying stimulus has several advantages that enable the effect of local vascular response delays to be overcome due to the mathematical properties of a sinusoid (Blockley et al., 2010). Transit and vascular response delays can be modelled as a phase shift of the inputted sinusoidal stimulus providing two major benefits. Firstly, the resulting BOLD response can be modelled as a sine wave with the same frequency as the stimulus and a local phase shift to correct for transit and vascular response delay at the voxel level. In this context the fitted amplitude of the sinusoid reflects CVR and the phase of the sinusoid provides similar timing information to TFA. Secondly, this means that a regressor based on end-tidal partial pressure of carbon dioxide (P_{ETCO_2}) is not required. This simplifies the estimation of CVR maps, since additional data does not need to be transferred to the analysis workstation, and may even provide the option of CVR map generation on the scanner. Furthermore, the sinusoidal stimulus protocol can be retrospectively reanalysed with fewer stimulus cycles, or fractions of cycles, to examine the effect of reducing scan time, since it is not the duration of the stimulus that is important but the stimulus frequency. Finally, because sinusoidal stimuli are smoothly varying they are less demanding for automated gas administration systems to generate and are likely to be more comfortable for participants as the peak carbon dioxide level is only experienced for one or two breaths in each cycle.

Therefore, the aim of this study was to develop a rapid CVR technique based on a sinusoidal hypercapnic stimulus. Comparison was made with a commonly applied block paradigm, which we term the Toronto protocol (Spano et al., 2012). Both protocols produce estimates of vascular reactivity and the timing of this reactivity, which to prevent ambiguity we describe as CVR magnitude and CVR phase, respectively. Firstly, estimates of CVR magnitude and CVR phase were compared for the Toronto and Sinusoid protocols with the same scan duration. Secondly, the

amount of data included in the analysis of the Sinusoid protocol was progressively reduced to investigate how rapidly CVR information can be acquired.

2. Methods

2.1. Imaging

All imaging was performed on a Siemens Prisma 3T scanner (Siemens Healthineers, Erlangen, Germany) using the body transmit coil and the vendors 32-channel receive coil. This study was approved by the Central University Research Ethics Committee (CUREC) at the University of Oxford. Ten healthy volunteers (age range 19–21, 5 female) were recruited and informed written consent obtained. Functional imaging consisted of BOLD-weighted EPI images with the following pulse sequence parameters: repetition time (TR) 2 s, echo time (TE) 30 ms, field of view (FOV) 220 mm \times 220 mm, matrix 64 \times 64, slices 24, slice thickness 5 mm, slice gap 0.5 mm, flip angle 80°, GRAPPA 2. Each functional scan had a duration of 7 min, resulting in the acquisition of 210 imaging volumes. A field map was acquired using a 2D Fast Low Angle Shot (FLASH) method with the following parameters: TR 378 ms, TE1/TE2 4.92 ms/7.38 ms, FOV of 220 mm \times 220 mm, matrix 64 \times 64, slices 24, slice thickness 4.5 mm, slice gap 0.45 mm, flip angle 45°. Finally, a high resolution T₁-weighted structural image was acquired for each subject using a 3D Magnetisation Prepared Rapid Acquisition Gradient Echo (MPRAGE) pulse sequence (Mugler and Brookeman, 1990) with the following parameters: TR 1.9 s, TE 3.74 ms, FOV 174 mm \times 192 mm \times 192 mm, matrix 116 \times 128 \times 128, flip angle 8°, inversion time (TI) 904 ms.

Details on how to access the imaging data that underlies this study can be found in [Appendix A](#).

2.2. Respiratory stimulus

Hypercapnia challenges were delivered by a computer controlled gas blender (RespirAct™ Gen 3, Thornhill Research Inc., Toronto, Canada) that implements a prospective algorithm for the targeting of blood gases (Slessarev et al., 2007). Subjects were fitted with a sequential gas delivery (SGD) breathing circuit, which was sealed to the face using adhesive tape (Tegaderm, 3M Healthcare, St. Paul, Minnesota, USA) to prevent the entrainment of room air. Subjects were then asked to sit comfortably outside the scanner whilst the prospective algorithm was calibrated. The subject's specific resting end-tidal carbon dioxide and oxygen partial pressures (P_{ETCO_2} and P_{ETO_2} , respectively) were first determined by averaging the first ten or so breaths into the breathing mask. The calibration consisted of initiating a baseline targeted at the subject's specific resting P_{ETCO_2} and P_{ETO_2} . Initial estimates of the subject's VCO_2 and VO_2 (their resting production/consumption of CO_2/O_2) based on height, weight and age were refined until a constant baseline was achieved with minimal drift. A brief presentation of the sinusoidal hypercapnic stimulus was then administered to the subject to prepare them for the sensations they might encounter whilst in the scanner.

Gas stimulus protocols ([Fig. 1a](#)) were tailored to each subject's resting P_{ETCO_2} and P_{ETO_2} baselines. Modulations in P_{ETCO_2} were targeted relative to baseline, whilst P_{ETO_2} was targeted to remain constant at baseline throughout. The Toronto gas protocol consisted of two blocks of hypercapnia, each with step changes of +10 mmHg; one of 45 s duration and the other 120 s. The former was preceded by a 60 s baseline and the latter by a 90 s baseline, with a final baseline period of 105 s completing the 7 min protocol (Sobczyk et al., 2015). The sinusoidal gas protocol was composed of seven sinusoidal cycles, each with a period of 60 s. This was the minimum period we could achieve using the automated gas administration equipment and hence the highest frequency. Experimental noise is expected to be proportional to the reciprocal of frequency and hence a higher frequency stimulus is preferred to minimise the noise contribution. To produce a purely hypercapnic stimulus, i.e. only increases in

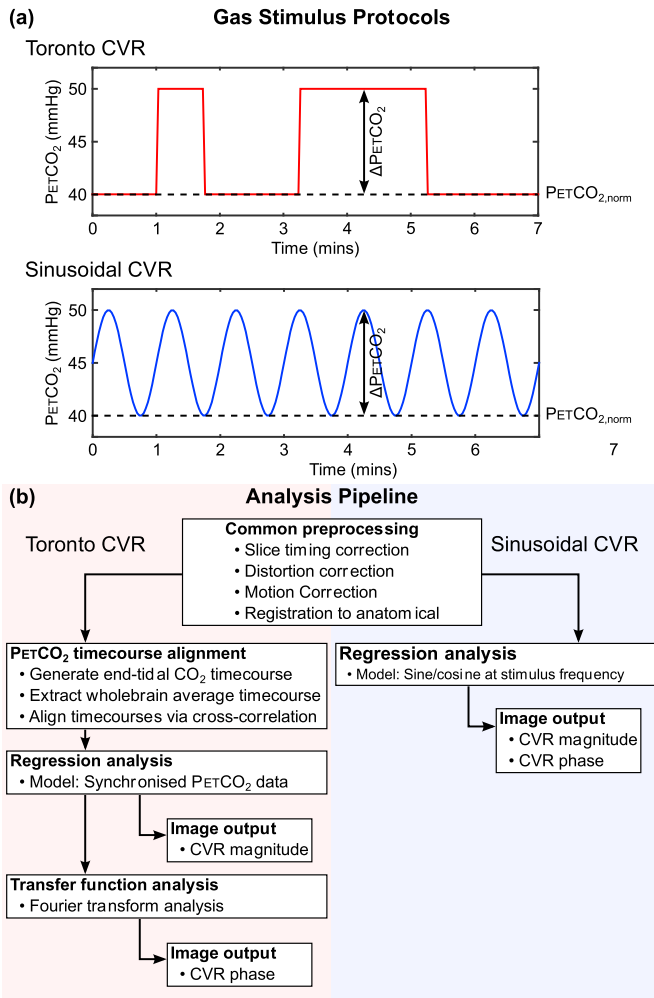


Fig. 1. Data analysis pipeline for Toronto and Sinusoid protocols. It is important for the end-tidal CO₂ regressor to be well-aligned with the BOLD data in the Toronto protocol to avoid underestimating changes in CVR Magnitude. The Sinusoid protocol analysis is inherently insensitive to such vascular response delays and does not require this step.

PETCO₂ from resting baseline, the amplitude was set to vary by ± 5 mmHg at +5 mmHg above resting baseline i.e. a variation in PETCO₂ from resting baseline to +10 mmHg (Fig. 1a). By spanning the same PETCO₂ range as the Toronto protocol, we aim to operate on the same portion of the vascular response curve. In this implementation, the prospective algorithm is very tolerant of increases in ventilation rate compared with the baseline level during calibration, but not reductions in ventilation. Therefore, subjects were coached to maintain their ventilation rate over the scanner intercom should it be observed to have dropped below baseline levels.

During the presentation of each 7 min stimulus protocol, imaging was performed using the 7 min BOLD-weighted EPI pulse sequence described above. Synchronisation of the respiratory and imaging protocols was manually initiated.

2.3. Image analysis

The basic image analysis pipeline is summarised in Fig. 1b. Imaging data from the two stimulus protocols were first submitted to a common pre-processing stage including motion correction (Jenkinson et al., 2002), fieldmap based EPI unwarping (Jenkinson et al., 2012), slice timing correction, removal of non-brain tissue (Smith, 2002) and spatial smoothing with a 5 mm FWHM kernel (Smith and Brady, 1997). High pass temporal filtering was also performed with cut-off values of 100 s (10 mHz) and 200 s (5 mHz) for the Sinusoid and Toronto protocols,

respectively. Images from the Toronto protocol were registered to MNI space via the subject's structural image (Greve and Fischl, 2009; Jenkinson et al., 2002). This registration was used to transform the MNI structural atlas (Mazziotta et al., 2001) and segmented structural images (Zhang et al., 2001) to functional space. Finally, the Sinusoid protocol images were registered to the Toronto protocol images.

The FMRIB Expert Analysis Tool (FEAT) was used to perform model-based multiple regression analysis (Woolrich et al., 2009). Motion parameters were not included in this analysis. For the Sinusoid protocol, the model was defined by sine and cosine terms with time periods of 60 s (equivalent to 16.7 mHz). This model is based on the observation that a cosine with arbitrary phase can be described by the sum of a sine and a cosine with equal frequency (ω), but different amplitudes (A and B). The amplitudes in Eq. (1) can be obtained from the GLM analysis.

$$A \cos(\omega t) + B \sin(\omega t) = \sqrt{A^2 + B^2} \cos[\omega t - \tan^{-1}(B/A)] \quad (1)$$

For the Toronto protocol, the model was defined by the measured PETCO₂ change during the challenge experienced by each subject. This PETCO₂ timecourse must first be synchronised with the associated BOLD signal changes in the brain, due to intersubject differences in blood arrival time. This was achieved by extracting the mean whole brain BOLD signal change, using the mask generated during the brain extraction process, and finding the maximum cross-correlation with the PETCO₂ data interpolated to the BOLD sampling frequency. High pass temporal filtering with the same cut-off as the imaging data was then applied and the temporal derivative included as an additional regressor.

From this analysis several outputs can be produced. Statistical maps were generated and thresholded at the voxel level with a corrected voxel P threshold of 0.05. The effect of the sine and cosine terms in the sinusoidal analysis were combined by using an F-test, whereas for the Toronto analysis a single T-test was used. Maps of CVR magnitude were calculated from the parameter estimates (PE) of the GLM analysis using Eq. (2) for the Sinusoid protocol and Eq. (3) for the Toronto protocol, where S_{mean} is the mean BOLD signal baseline and ΔPETCO_2 is the change in end-tidal partial pressure of CO₂. Normalisation by ΔPETCO_2 is included to control for difference in the stimulus magnitude across subjects.

$$\text{CVR}_{\text{sin}}^{\text{mag}} = \frac{\sqrt{PE_{\text{sin}}^2 + PE_{\text{cos}}^2}}{S_{\text{mean}} \Delta\text{PETCO}_2} \quad (2)$$

$$\text{CVR}_{\text{tor}}^{\text{mag}} = \frac{PE_{\text{PETCO}_2}}{S_{\text{mean}} \Delta\text{PETCO}_2} \quad (3)$$

Despite the use of a GLM analysis in this work, in contrast to the Fourier analysis used previously (Blockley et al., 2010), it is still possible to calculate maps of CVR phase from the sinusoidal protocol by using Eq. (4).

$$\text{CVR}_{\text{sin}}^{\text{pha}} = \tan^{-1} \frac{PE_{\text{sin}}}{PE_{\text{cos}}} \quad (4)$$

To provide CVR phase estimates that are comparable with the Toronto protocol, maps were produced using the whole brain phase as a reference i.e. equivalent to the synchronisation performed for the Toronto protocol. This was achieved by extracting a whole brain BOLD signal timecourse and estimating the CVR phase using Eq. (4). This global phase value was then subtracted from the CVR phase estimates from each voxel.

For the Toronto protocol Transfer Function Analysis (TFA) (Duffin et al., 2015) was used to estimate CVR phase. Since this is a Fourier based method, and as such no standard tools exist, it was implemented in MATLAB (Mathworks, Natick, MA, USA). The normalised transfer function $H(f)$ is calculated by dividing the cross power spectral density (CPSD) of the BOLD and PETCO₂ timecourses by the power spectral density (PSD) of the BOLD timecourse. Both the BOLD and PETCO₂

timecourses were demeaned prior to spectral analysis.

$$H(f) = \frac{CPSD_{BOLD, PETCO_2}(f)}{PSD_{BOLD}(f)} \quad (5)$$

CVR phase can be calculated from the real and imaginary parts of $H(f)$, denoted by subscript r and i , at the frequency of interest. Previously this was selected as 10 mHz, which had been found to be the frequency with the highest coherence (Duffin et al., 2015). However, in order to enable comparison with the Sinusoid protocol, 16.7 mHz was used in this study. Coherence analysis of the whole brain BOLD signal with the $PETCO_2$ recording reveals that this results in only a small reduction in coherence (Fig. S1).

$$CVR_{tor}^{pha} = \tan^{-1} \frac{H(f)_i}{H(f)_r} \quad (6)$$

The use of a GLM analysis also enables the errors in measurements of CVR magnitude and CVR phase to be estimated. This can be achieved by propagating the errors in the GLM parameter estimates and residuals through to the final CVR estimate. The standard deviation in the CVR magnitude ($\sigma_{CVR_X^{mag}}$) can be calculated using Eq. (7), where PE_X and $\sigma_{PE_X}^2$ are the parameter estimate and the variance in that estimate for protocol X and $\sigma_{S_{mean}}^2$ is the variance in the mean BOLD signal baseline.

$$\sigma_{CVR_X^{mag}} = \frac{PE_X}{S_{mean}} \sqrt{\frac{\sigma_{PE_X}^2}{PE_X^2} + \frac{\sigma_{S_{mean}}^2}{S_{mean}^2}} \quad (7)$$

Since the Sinusoid protocol uses a pair of parameter estimates to calculate CVR magnitude the variance in those estimates must first be combined using the equation below before application of Eq. (7), where $\sigma_{PE_{sin}}^2$ and $\sigma_{PE_{cos}}^2$ are the variance in the sine and cosine parameter estimates.

$$\sigma_{PE_{sin/cos}}^2 = \frac{PE_{sin}^2}{PE_{sin}^2 + PE_{cos}^2} \sigma_{PE_{sin}}^2 + \frac{PE_{cos}^2}{PE_{sin}^2 + PE_{cos}^2} \sigma_{PE_{cos}}^2 \quad (8)$$

However, the absolute error in CVR magnitude does not take into account the large differences in the scale of CVR magnitude particularly between grey and white matter. Under these conditions it is preferable to represent the standard deviation as a fraction of CVR magnitude by calculating the relative standard deviation (RSD). It should be noted that the calculation of RSD is the same as for coefficient of variation. However, the coefficient of variation is usually calculated as the standard deviation over the mean of repeated measurements. Since here we calculate the ratio of the error in the parameter over its value we use the term RSD to reduce ambiguity.

$$RSD_{CVR_X^{mag}} = \frac{\sigma_{CVR_X^{mag}}}{CVR_X^{mag}} \quad (9)$$

Estimating the variance in the CVR phase measurement was only possible for the Sinusoid protocol due to the use of TFA in the Toronto protocol.

$$\sigma_{CVR_{sin}^{pha}} = \frac{1}{1 + PE_{sin}^2/PE_{cos}^2} \sqrt{\frac{\sigma_{PE_{sin}}^2}{PE_{cos}^2} + \frac{\sigma_{PE_{cos}}^2}{PE_{sin}^2}} \quad (10)$$

Details of how to access the code that was used to perform this analysis can be found in Appendix A.

2.4. Stimulus performance

The normocapnic baseline $PETCO_2$ ($PETCO_{2,norm}$) and the difference between this baseline and the peak change in $PETCO_2$ ($\Delta PETCO_2$), i.e. the range of $PETCO_2$ change, were measured for each protocol and subject (Fig. 1a). First, the automated end-tidal picking routine was manually

inspected and corrected where necessary, using software provided with the RespirAct, to ensure accurate $PETCO_2$ estimation. Linear regression was then performed using a prototypical model of the stimulus (i.e. a boxcar temporally aligned with the $PETCO_2$ data or a sine/cosine pair at 16.7 mHz consistent with the Sinusoid protocol's image analysis model based on Eq. (1)) and a constant term. For the Toronto protocol, the boxcar represents $\Delta PETCO_2$ and the constant term represents $PETCO_{2,norm}$. However, for the Sinusoid protocol the modulus of the sine/cosine pair gives the amplitude of the sine wave stimulus and the constant term gives the baseline of this sine wave. Therefore, in order to report the range of $PETCO_2$ change consistently, $\Delta PETCO_2$ is calculated as twice the amplitude of the sine wave and $PETCO_{2,norm}$ is the value of the sine wave baseline minus the amplitude of the sine wave stimulus (Fig. 1a).

2.5. Comparison between Toronto and Sinusoid protocols

Investigations were made to compare the sensitivity and equivalence of the two protocols. Firstly, the number of statistically significant voxels that passed the corrected voxel level threshold (GRF-theory-based maximum height thresholding at $p < 0.05$) were counted for each subject and protocol. In order to control for potential differences in subject motion between protocols the mean motion as calculated during the motion correction step was extracted (Jenkinson et al., 2002). Mean motion represents the mean-root-mean square displacement between adjacent time points and has been shown to be associated with reduced temporal signal to noise ratio (SNR) in fMRI experiments (Van Dijk et al., 2012). It is important that the effective temporal SNR is consistent across protocols in order to isolate the effect of different stimulus paradigm rather than difference in noise characteristics.

Next the equivalence of the CVR estimates produced by the Toronto and Sinusoid protocols was explored. A grey matter ROI was defined based on the grey matter segmentation thresholded at a partial volume estimate of 0.5. Values of CVR magnitude and phase were extracted from each subject using this ROI definition. CVR phase values were corrected to the mean grey matter phase value to provide a consistent reference across methods. Furthermore, wrapped phase values were discarded from the analysis by considering whether the difference between any two values for a given voxel was greater than $\pm\pi$, which suggests that the phase value is wrapped in one protocol but not the other. Systematic differences between the estimates of CVR magnitude and phase from each of the protocols were assessed by fitting a simple model: linear slope (m) and intercept (c). For the CVR magnitude data, a χ^2 fit with variance in the estimates from both protocols was performed by minimising Eq. (11) to prevent bias (Press, 2007). Variance information was provided by Eqs. (7) and (8).

$$\sum \frac{[CVR_{sin}^{mag} - (m CVR_{tor}^{mag} + c)]^2}{\sigma_{CVR_{sin}^{mag}}^2 + m^2 \sigma_{CVR_{tor}^{mag}}^2} \quad (11)$$

However, this approach was not possible for the CVR phase data as the variance could only be calculated for the Sinusoid protocol. Simple linear regression is not valid in this case because it would implicitly attribute all of the variance to one of the protocols. Therefore, orthogonal regression (minimising Eq. (12)) was used whereby the variance in both methods was assumed to be equal i.e. rather than calculate the vertical distance from the point to the line, orthogonal regression calculates the diagonal to the line.

$$\sum \frac{[CVR_{sin}^{pha} - (m CVR_{tor}^{pha} + c)]^2}{1 + m^2} \quad (12)$$

For both CVR parameters, magnitude and phase, the estimates are equivalent if $m \approx 1$ and $c \approx 0$. Finally, the importance of accounting for local vascular delays in the Sinusoid protocol was considered. Rather than use the sine/cosine model, a $PETCO_2$ regressor was created using the same approach as the Toronto protocol. Comparison was then made with

the Toronto protocol to assess whether the CVR magnitude estimates were equivalent.

2.6. Effect of reducing Sinusoid protocol scan duration

The effect of reducing the amount of data used to measure the CVR parameters using the Sinusoid protocol was explored. This was achieved by truncating the data set at scan durations between 1 min (30 vol) and 6 min (150 vol) in steps of 1 min (30 vol). The full analysis, including pre-processing and GLM analysis, was performed for each truncated dataset, and maps of CVR magnitude and phase were generated. High pass temporal filtering at 100 s was disabled for the 1 min scan duration.

The impact of scan time reduction was investigated at the level of whole brain grey matter. An ROI was generated based on voxels in the Toronto protocol that met the statistical threshold and was then refined using a grey matter mask (grey matter segmentation partial volume estimate thresholded at 0.5). The mean and standard deviation of the CVR magnitude and phase values in this ROI were calculated for each scan duration and subject. In addition, the number of statistically significant voxels from the GLM analysis were calculated for each scan duration and subject. These results were subjected to a two-way ANOVA test to investigate the null hypothesis that the group mean values were equal. In the case that the group mean values were found to be significantly different, pairwise comparison was performed using the Tukey-Kramer method (honest significance difference test) to consider which pairs of group means were significantly different. The Tukey-Kramer method controls for multiple comparisons by correcting for the family wise error rate. In this sense it is less conservative than multiple T-tests with Bonferroni correction.

3. Results

Both stimulus protocols yielded reliable and accurate respiratory challenges. Table 1 details this performance by listing the baseline PetCO_2 and stimulus induced ΔPetCO_2 . Although within the accuracy of the end-tidal gas targeting system, on average baseline PetCO_2 was 0.9 mmHg higher and ΔPetCO_2 was 0.7 mmHg lower for the Toronto protocol compared with the Sinusoid protocol. Paired two tailed T-tests showed that these differences were significant at $p < 0.001$ and $p < 0.01$, respectively. Although the target of 10 mmHg PetCO_2 change was not attained, all subjects experienced similar PetCO_2 changes within a standard deviation of 1.2 mmHg. The mean PetCO_2 change as a function of time, and the standard deviation, across subjects can also be found in the supplemental data, alongside the mean grey matter and white matter BOLD signal change (Fig. S2).

In order to compare the sensitivity of the two protocols the number of voxels that passed the voxel level statistical threshold were counted. Table 2 displays these results for the full 7 min data sets, as well as two

examples of the truncated Sinusoid protocol data. The mean motion is also tabulated here to demonstrate the impact of motion on the statistical maps. Mean motion is fairly consistent between protocols and truncated data sets, with one exception. Subject 10 shows considerably higher mean motion for the full Sinusoid protocol compared with the Toronto protocol or truncated data sets. Further investigation revealed large translations in the last two stimulus cycles. Since this would lead to a varying error contribution in the GLM analysis across truncated data sets, this subject was excluded from further analysis. For the remaining subjects, a paired two-tailed T-test showed that the number of statistically significant voxels was insignificantly different between the Toronto and Sinusoid protocols ($p = 0.36$).

Examples of the main outputs of the analysis are displayed for both protocols in Fig. 2, consisting of unthresholded Z-statistic maps, CVR magnitude, CVR magnitude RSD, CVR phase and CVR phase standard deviation (SD). Both protocols can be seen to produce qualitatively similar results. A reduced Z-statistic value is observed in the Sinusoid protocol compared with the Toronto protocol (Fig. 2a/e). However, similar grey matter to white matter contrast is observed across CVR magnitude (Fig. 2b/f) and phase (Fig. 2d/h) maps. Similarly estimates of the error in these parameters demonstrate increased variance in white matter compared with grey matter. To investigate the quantitative equivalence of the protocols estimates of CVR magnitude and CVR phase were plotted on a voxel-by-voxel basis for each subject. Fig. 3a and d shows an example subject for CVR magnitude and phase, respectively. Per subject estimates of the slope and intercept for CVR magnitude reveal that the group mean slope (1.05 ± 0.11 , mean \pm s.d.) is not significantly different from unity ($p = 0.24$, Fig. 3b), but the group mean intercept (0.03 ± 0.03) is significantly different from zero ($p < 0.05$, Fig. 3c). For CVR phase the group mean slope (0.64 ± 0.17) and intercept (0.05 ± 0.05) are significantly different from unity and zero, respectively, at $p < 0.05$. Further comparison of the Toronto protocol with the Sinusoid protocol analysed using a PetCO_2 regressor in the same manner as the Toronto protocol was also performed (Fig. S3). Under these conditions the estimates of CVR magnitude were not found to be equivalent with group mean slope (0.51 ± 0.16) and intercept (0.00 ± 0.01) being significantly different ($p < 0.05$) from unity and zero, respectively.

An example of the effect of reducing scan duration is displayed in Fig. 4. Two examples of the truncated Sinusoid protocol (5 min and 3 min) are presented alongside the full 7 min acquisition. Values of the Z-statistic can be seen to reduce with the amount of data included in the analysis (Fig. 4a–c). CVR magnitude maps look qualitatively very similar across scan durations (Fig. 4d–f), whilst CVR phase maps show some small differences when only 3 min of data are used (Fig. 4g–i). This is further explored across all subjects in Fig. 5. The group mean of the mean CVR magnitude across the ROI (Fig. 5a) was seen to increase slightly with reduced scan time. A two-way ANOVA test showed that not all group means were equal ($p < 0.001$), but a paired multiple comparisons analysis showed that only the 1 min duration was significantly different ($p < 0.001$) to the full data set. A similar increase was observed for the group mean standard deviation of the CVR magnitude (Fig. 5b). Again group means were not all equal ($p < 0.001$) and only the 1 min duration was significantly different ($p < 0.001$) to the full data set. The group mean of the mean CVR phase displayed little variation (Fig. 5c) and was not significant ($p = 0.99$). The group mean of the standard deviation of the CVR phase showed the largest increase with time reduction (Fig. 5d). The group means were significantly different ($p < 0.001$) and the 1 min ($p < 0.001$) and 2 min ($p < 0.01$) scan durations were significantly different to the full data set. The group mean number of statistically significant voxels (Fig. 5e) reduced with scan time and were significantly different ($p < 0.001$). Pairwise comparison revealed significant differences between the 1, 2 and 3 min durations ($p < 0.001$) and the full data set. Finally, for comparison Fig. 5f scales the group means of the standard deviation of the CVR magnitude and phase to the full data set, demonstrating a larger effect of scan time reduction on CVR phase than CVR magnitude.

Table 1

Respiratory stimulus performance across protocols as defined by baseline normocapnic PetCO_2 ($\text{PetCO}_{2,\text{norm}}$) and the change in PetCO_2 due to the stimulus (ΔPetCO_2).

Subject ID	Toronto protocol		Sinusoid protocol	
	$\text{PetCO}_{2,\text{norm}}$	ΔPetCO_2	$\text{PetCO}_{2,\text{norm}}$	ΔPetCO_2
01	38.6	7.0	37.8	7.9
02	37.9	7.1	37.1	8.0
03	43.1	6.2	41.9	6.9
04	43.8	5.0	42.2	5.9
05	40.4	7.4	39.5	7.5
06	31.0	6.0	29.9	6.6
07	41.2	5.3	40.5	6.2
08	40.6	7.9	40.0	8.0
09	38.7	8.0	38.5	8.5
10	38.7	7.7	37.4	9.7
Mean	39.4	6.8	38.5	7.5
SD	3.5	1.1	3.5	1.2

Table 2

Number of voxels above the voxel level statistical threshold for the 7 min datasets of each protocol and the Sinusoid protocol truncated at 5 min and 3 min. The mean motion, defined as average root mean square displacement between adjacent time points, for each data set is presented alongside voxel count to highlight the effect of subject motion.

Subject ID	Toronto protocol		Sinusoid protocol					
	7 min		7 min		5 min		3 min	
	#voxels	Motion	#voxels	Motion	#voxels	Motion	#voxels	Motion
01	18995	0.11	17089	0.10	14735	0.10	10345	0.11
02	15650	0.13	17054	0.10	15969	0.10	15380	0.11
03	17820	0.14	15104	0.15	14221	0.14	13695	0.13
04	9590	0.20	10174	0.20	8736	0.20	5013	0.19
05	16828	0.09	17185	0.09	15764	0.09	13941	0.09
06	5090	0.27	7106	0.29	6895	0.29	4785	0.22
07	15507	0.20	14643	0.24	12490	0.22	12081	0.21
08	19356	0.23	12400	0.30	10986	0.32	8070	0.34
09	19333	0.08	19507	0.12	17852	0.12	15109	0.10
10	19630	0.19	6767	0.40	15776	0.21	12890	0.22
Mean	15780	0.16	13703	0.20	13343	0.18	11131	0.17
SD	4814	0.06	4437	0.11	3509	0.08	3945	0.08

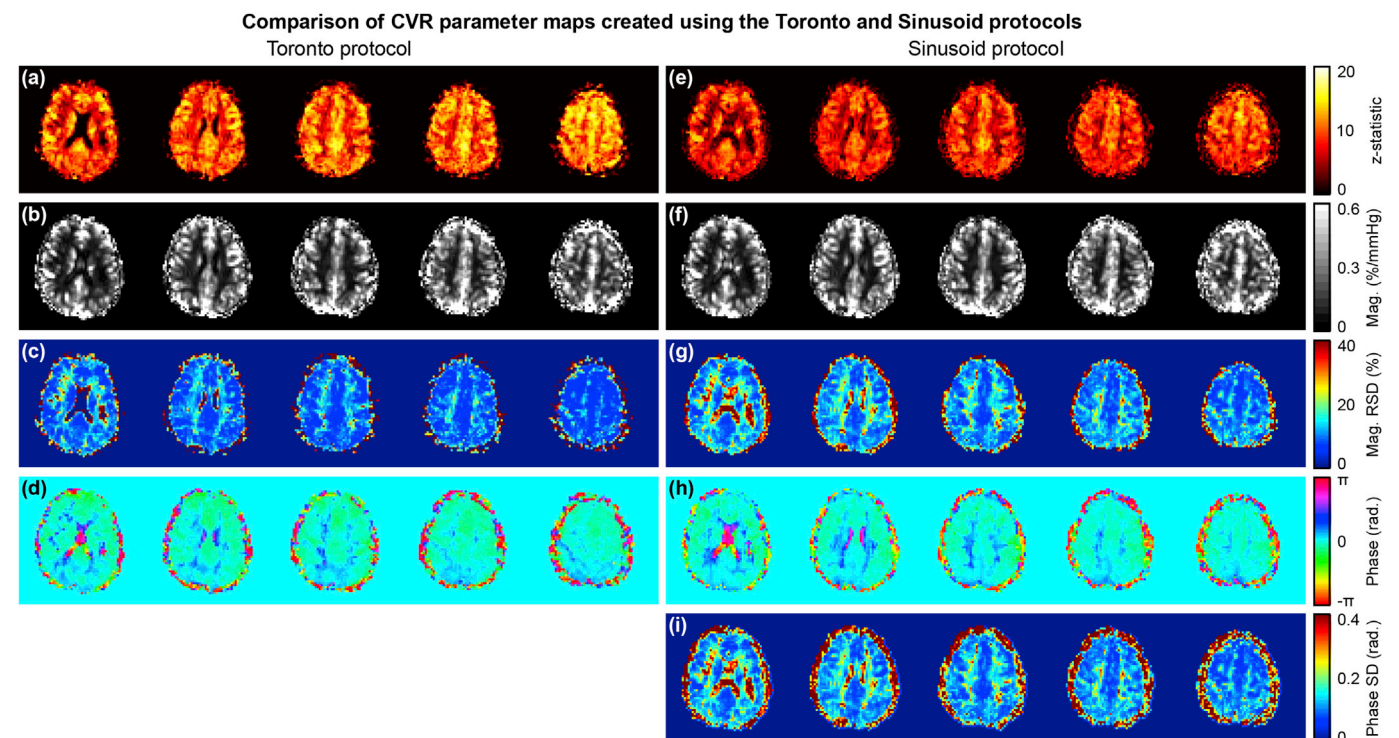


Fig. 2. Example CVR maps from a single subject (Subject 01). A subset of five contiguous slices are displayed superior to the lateral ventricles. Maps (a)–(d) were produced using the Toronto protocol and (e)–(i) using the Sinusoid protocol. Maps were generated to display (a/e) statistical correlation with the CO₂ stimulus (Z-statistic), (b/f) CVR magnitude (normalised by the change in $P_{ET}CO_2$), (c/g) relative standard deviation (RSD) of the CVR magnitude estimate, (d/h) CVR phase and (i) standard deviation of the CVR phase estimate. Note: It is not possible to generate maps of the error in CVR phase for the Toronto protocol.

4. Discussion

CVR mapping using MRI is a promising clinical tool for stress testing cerebral blood vessels. However, there are several aspects of current CVR mapping techniques that limit their clinical application. In this study we concentrated on minimising the scan duration in order to improve the compatibility of this technique with clinical workflows. By utilising a sinusoidally modulated hypercapnia challenge we were able to retrospectively examine the effect of reducing the scan duration. In turn we were able to demonstrate that good quality CVR maps can be acquired in around 3 min, rather than the more typical 7 min. Furthermore, we demonstrated that CVR magnitude maps generated using this sinusoidal stimulus are equivalent to the more conventional block paradigm.

4.1. Stimulus performance

Gas stimulus protocols were tailored to each subject's individual baseline $P_{ET}CO_2$. This baseline was maintained within 1 mmHg between the protocols, but was statistically significantly different none the less. The temporal characteristics of the stimuli were well reproduced for both protocols (Fig. S2). Since the vascular response to carbon dioxide is sigmoidal in form in healthy subjects (Bhogal et al., 2014) it is possible that the two protocols were performed on different parts of the sigmoid curve. However, in practice maintaining baseline $P_{ET}CO_2$ to a higher accuracy than 1 mmHg is challenging. Both stimulus protocols elicited $P_{ET}CO_2$ changes of the order of 7 mmHg, which should place the vascular response within the linear regime of the sigmoidal vascular response (Bhogal et al., 2014). A statistically significant difference in $\Delta P_{ET}CO_2$ was

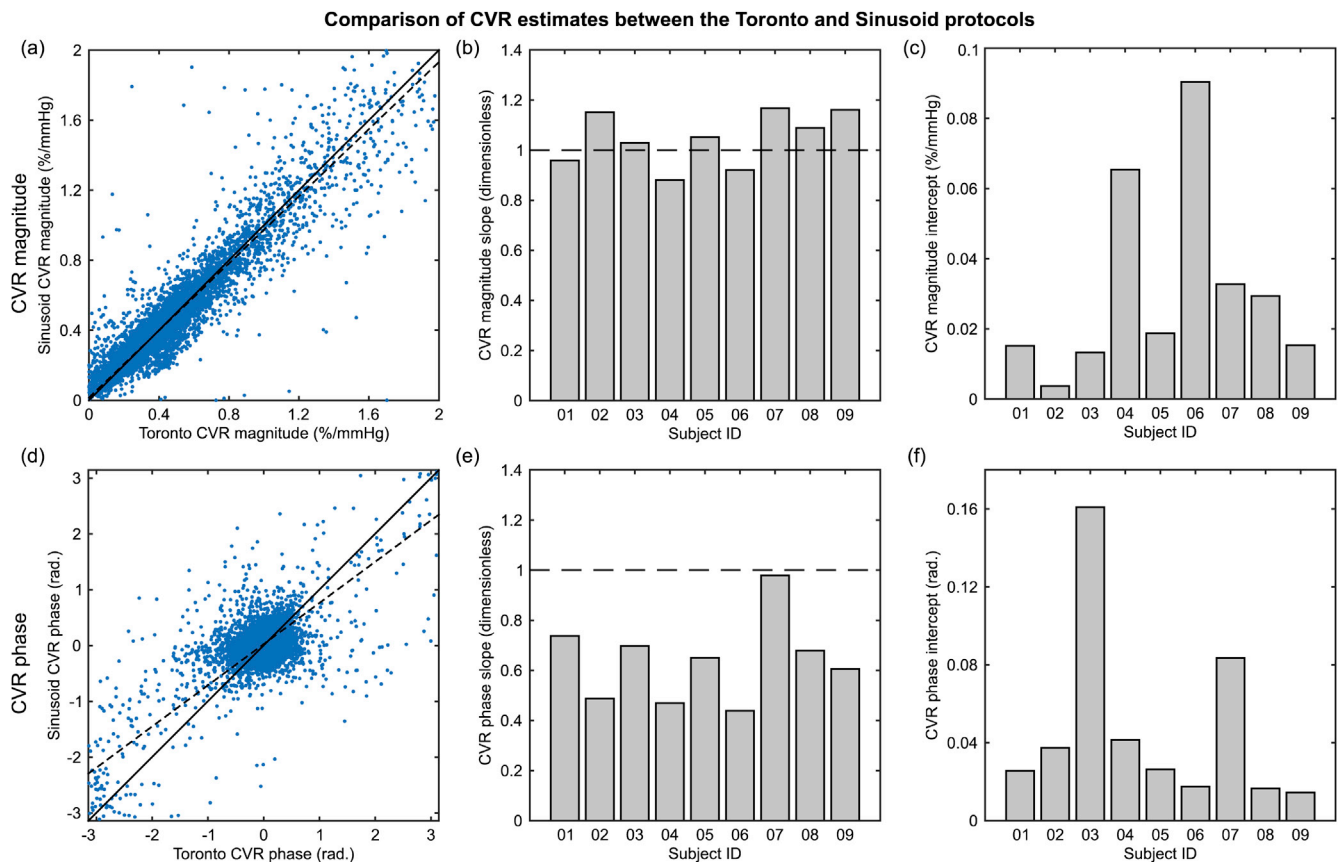


Fig. 3. Estimates of (a) CVR magnitude and (d) CVR phase were compared on a voxel-by-voxel basis for each subject (single example subject shown). The slope and intercept of this relationship were estimated (plotted as a dashed line and compared to the solid line of unity). For CVR magnitude, the mean slope (b) was not significantly different to unity, suggesting the protocols give equivalent estimates. However, the intercept (c) was found to be significantly different to zero ($p < 0.05$), resulting in a mean intercept of $0.03\%/mmHg$. For CVR phase, the mean slope (e) was significantly different to unity ($p < 0.05$), indicating that these measures are not equivalent, whilst the intercept (f) was not significantly different from zero.

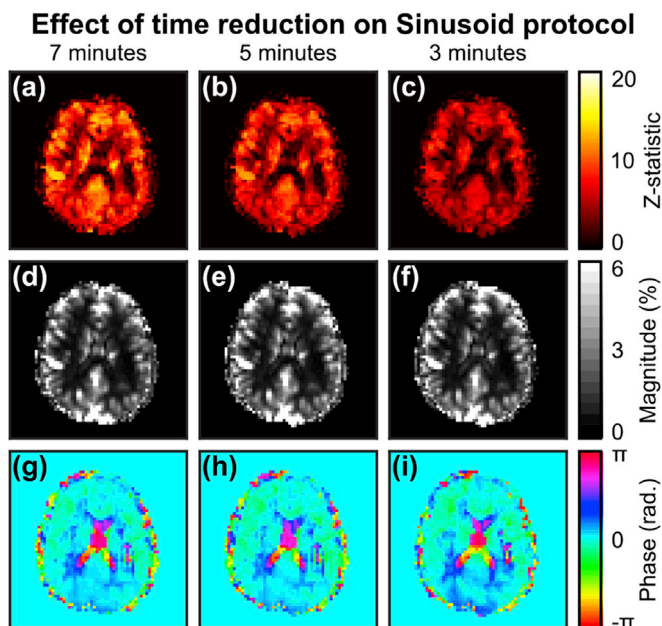


Fig. 4. Example single slice of CVR maps from the Sinusoid protocol as scan duration is reduced (Subject 01) for (a)–(c) statistical correlation, (d)–(f) CVR magnitude and (g)–(i) CVR phase.

observed, although well within the accuracy of the gas delivery system at 0.7 mmHg . Since CVR magnitude values are normalised by ΔP_{ETCO_2} this

should not produce a bias between the protocols. Unfortunately, subject tolerance of both stimulus protocols was not recorded. However, none of the subjects reported discomfort from either stimulus protocol.

4.2. Comparison between Toronto and Sinusoid protocols

Before discussing the results of the protocol comparison it is useful to consider the advantages and disadvantages of the two stimulus protocols. As a more conventional block paradigm, the Toronto protocol is an easier stimulus to implement. However, synchronisation of the measured P_{ETCO_2} experienced by the subject with the BOLD data is critical to the accurate estimation of magnitude of the CVR change. Whilst this is practical when synchronising with the whole brain average BOLD signal, the presence of local variations in vascular response delay open up the possibility of the underestimation of CVR magnitude, or the measurement of spurious negative signal changes (Duffin et al., 2015). This can be mitigated by the use of long blocks of hypercapnia, but therefore limits how short the total acquisition can be. In contrast sinusoidal stimuli have seen only limited application (Driver et al., 2015). To be clinically practical, computer controlled gas delivery is desirable, although a manual implementation has also been demonstrated (Liu et al., 2016). In the previous implementation a Fourier analysis approach was used based on in-house analysis software (Blockley et al., 2010). However, in this study we reframe the analysis in order to use free and widely available fMRI analysis tools (Jenkinson et al., 2012). One of the inherent advantages of the Sinusoid protocol is its insensitivity to local vascular response delays. This is due to the fact that any sinusoid with arbitrary amplitude and phase can be represented by the sum of a sine and a cosine with different amplitudes (Eq. (1)). In this context only the frequency of

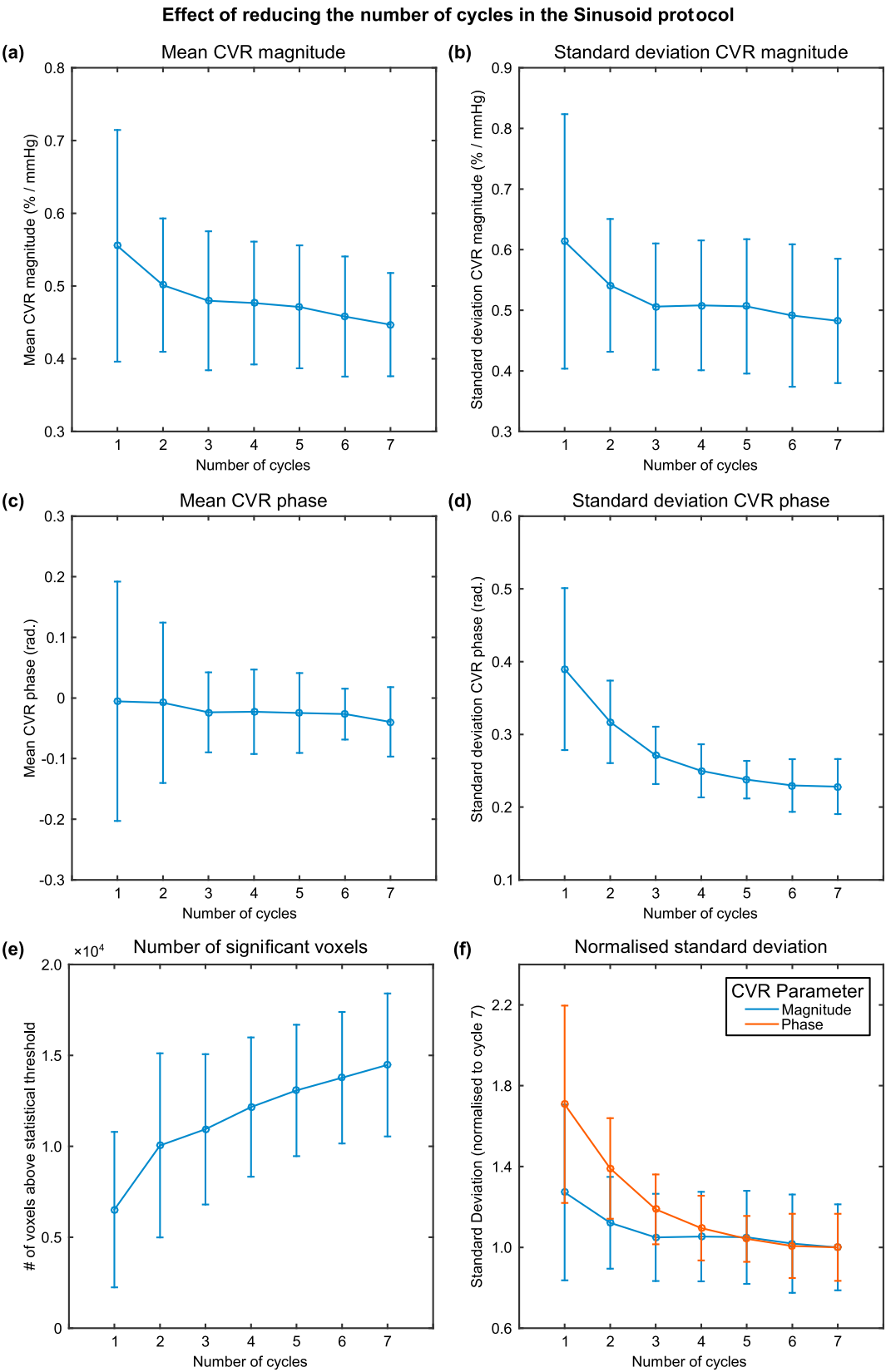


Fig. 5. Analysis of the effect of reducing the scan duration of the Sinusoid protocol for (a/b) CVR magnitude, (c/d) CVR phase and (e) the number of voxels above the voxel level statistical threshold. Analysis was performed for a grey matter region of interest (ROI) where the mean and standard deviation of the estimates within the ROI were calculated. The standard deviation of the CVR magnitude and phase are compared directly (f) by normalising to the 7 min scan duration.

the stimulus is important, rather than the timing. This enables the short time period stimuli used in this work, which would otherwise result in underestimates, or artefactual negative values, of CVR magnitude. Negative values could be caused by very long combined transit and vascular delays, for instance in the case of collateral flow in disease, leading to positive increases in flow that are in anti-phase with the stimulus. Finally, simple sine and cosine functions were used as regressors in the GLM analysis, rather than the measured PETCO_2 time-course. Despite this, the number of statistically significant voxels (Table 2) was not significantly different to the Toronto protocol across the group. This approach simplifies the analysis as the PETCO_2 data does not need to be transferred to the analysis computer and synchronised with the BOLD data. However, it should be noted that the PETCO_2 regressor for the Toronto protocol was aligned with the global brain signal and therefore, unlike the Sinusoid protocol, voxel level correction for delays was not performed. It is possible this could have resulted in fewer significant voxels, however, large deviations from the global brain signal delay within grey matter are unlikely in this healthy cohort, although the variations between grey and white matter still have the potential to be large. Delays of this magnitude are accounted for in the analysis of the Sinusoid protocol. However, the maximum time delay that can be tolerated by this protocol is determined by the time period of the stimulus. In this case relative delays over 60 s will result in phase wrapping meaning that such delays are indistinguishable from no delay. Larger delays can be measured by using a stimulus with a longer time period. In addition, the symmetric nature of the sinusoidal stimulus means anti-phase responses to the stimulus cannot be distinguished from negative responses using the current analysis approach. This is one of the advantages of the asymmetric Toronto protocol. However, such information can in theory be extracted from the Sinusoid protocol using a model based analysis incorporating an initial delay at baseline to reflect the increased vascular response time.

Maps of CVR magnitude were found to have qualitatively similar features (Fig. 2b/f). Furthermore, quantitative analysis comparing CVR magnitude on a voxel-by-voxel basis (Fig. 3a) showed that the slope between the protocols was not significantly different to unity (Fig. 3b), but that the intercept was significantly different from zero (Fig. 3c). This can be interpreted as a constant offset, or bias, of 0.03%/mmHg. However, this is unlikely to have a practical impact on maps of CVR magnitude. By utilising estimates of the variance in the parameter estimates and the residuals from the GLM analysis it was possible to evaluate the standard deviation of the CVR magnitude measurement. By presenting this as the relative standard deviation (RSD), with respect to the mean, the large degree of heterogeneity in CVR magnitude is controlled, revealing more noisy estimates in white matter (Fig. 2c/g). However, the standard deviation in CVR magnitude, as estimated using Eq. (7), should be viewed with caution as it relies on the variance in S_{mean} from the residuals. The residuals include contributions from motion and physiological noise that aren't included in the GLM model. Therefore, large amounts of motion will result in larger values of RSD, in effect being categorised as noise.

The importance of accounting for local delays was also demonstrated by analysing the Sinusoid protocol in the same manner as the Toronto protocol i.e. using a time aligned PETCO_2 regressor. Using the same analysis as Fig. 3, but only for CVR magnitude, revealed that the slope and gradient relationship with the Toronto protocol (Fig. S3) were significantly different to unity and zero, respectively. This suggests that the CVR magnitude estimates are not equivalent. Since the PETCO_2 regressor was only aligned to the global signal, local vascular response delays were not accounted for. Such delays are a significant fraction of the stimulus duration for shorter stimuli, resulting in an underestimate of the CVR magnitude. However, this is not an issue specific to the Sinusoid protocol, but is likely to be encountered with any short time period stimulus. Since short stimuli are required to reduce scan duration, it is important to ensure this is adequately accounted for.

Maps of CVR phase also showed clear similarities between methods

(Fig. 2d/h). Quantitative analysis was performed on a voxel-by-voxel basis (Fig. 3d). However, the slope was found to be significantly different to unity (Fig. 3e), suggesting that the estimates of the two protocols are not equivalent. Values of the intercept were not significantly different to zero. This disparity may be due to the large difference in stimulus duration between the Toronto (45–120 s above baseline PETCO_2) and the Sinusoid protocol (30 s above baseline PETCO_2 in each 60 s cycle). Due to the more sustained nature of the Toronto protocol the vascular response is likely to reach a new steady state, enabling vascular steal effects to manifest in disease. In contrast the shorter stimulus duration of the Sinusoid protocol may not allow such steal effects to be revealed. Therefore, further optimisation of the time period of the Sinusoid stimulus is required in a patient cohort. However, this frequency dependence of the CVR response may also provide an additional window on the underlying vascular physiology.

Maps of the standard deviation of the CVR phase measurement were estimated for the Sinusoid protocol by propagating the errors in the parameter estimates (Fig. 2i). RSD was not used because of the relative nature of phase i.e. the reference phase is arbitrary. It is not possible to estimate the standard deviation of the Toronto CVR phase due to the use of TFA, although an analysis of the effects of noise was included in the original paper (Duffin et al., 2015).

4.3. Effect of reducing Sinusoid protocol scan duration

Rather than acquire multiple scans with different durations, the same 7 min protocol was truncated to investigate the effect of reducing scan duration. From a qualitative perspective, whilst the values of the Z-statistic are reduced with decreasing scan duration, there appears to be relatively little effect on maps of CVR magnitude at scan durations of 3 or 5 min, and only small differences in the 3 min CVR phase map (Fig. 4). Quantitative analysis confirmed that the number of above threshold voxels in the Z-statistic maps was significantly different in the 1, 2 and 3 min scan durations when compared with the full data set. Furthermore, the results in Fig. 5e are consistent with the expected reduction in sensitivity demonstrated for fMRI analysis (Murphy et al., 2007). CVR magnitude was only minimally affected, consistent with the qualitative assessment above, with only the 1 min scan duration found to be significantly different to the full data set for both the mean and standard deviation across the ROI. Estimates of CVR phase appear to be more strongly affected by scan time reduction. Whilst the mean over the ROI was not significantly different as a function of scan duration, the standard deviation was significantly different for the 1 and 2 min durations. This increased sensitivity of CVR phase to scan time reduction, relative to CVR magnitude, was highlighted by normalising Fig. 5b and d to their 7 min values. The standard deviation of CVR phase over the ROI clearly increases much more rapidly for CVR phase than CVR magnitude, necessitating longer scan duration where CVR phase is a priority. In summary, the results would suggest that scan time could be reduced to be in the range of 3–5 min with minimal effect on the resulting maps of CVR.

4.4. Limitations and future work

In the current implementation of this technique, long patient preparation times remain the largest barrier to clinical adoption. Whilst it was not the aim of this study to tackle this problem, it does deserve further consideration. To maintain a constant PETCO_2 baseline with minimal drift using the prospective end-tidal gas targeting system used in this study, the system must be calibrated to each individual. In our hands this process takes about 30 min, including application of the mask, although it may be shorter for more experienced users. However, there is a great deal of scope for time reduction by automating this calibration step, which will likely be implemented in future hardware developments. In the short term, using the current hardware, it should still be possible to realise shorter patient preparation times, albeit at the expense of a small amount of PETCO_2 baseline drift. As noted above, the gas targeting system

provides an initial setup based on the height, weight and age of the subject. The calibration process enables this setup to be refined. However, the initial estimate results in only small amounts of drift in many cases. Small amounts of drift are removed by the high-pass temporal filter and will not affect estimates of CVR so long as the vasculature remains in the linear regime of the sigmoidal vascular response. Further work is required to investigate this approach.

It also wasn't possible to examine the hypothesis that the Sinusoid protocol should be better able to account for local variations in vascular response delay using the data from this healthy cohort. Data acquired in patients where long transit or vascular response delays will be required to confirm this.

5. Conclusions

In this study we have demonstrated that a sinusoidal hypercapnia stimulus provides equivalent information about CVR to a conventional block paradigm. Furthermore, we have shown that the scan duration of the Sinusoid protocol can be drastically reduced with only a small effect on the resulting CVR maps. This development should enable scan durations between 3 and 5 min and has the potential to enable more widespread clinical adoption.

Acknowledgements

This work was supported by the Engineering and Physical Sciences Research Council [grant number EP/K025716/1]. DPB also received salary support from Cancer Research UK.

Appendix A. Supplementary data

The raw data that underpins this work can be accessed via the Oxford Research Archive repository, doi: <https://doi.org/10.5287/bodleian:Xk48adQAO>. Furthermore, the code to perform the analyses on these data can be accessed via the Zenodo repository, doi: <https://doi.org/10.5281/zenodo.495612>. Supplementary data related to this article can be found at <http://dx.doi.org/10.1016/j.neuroimage.2017.07.048>.

References

- Bhogal, A.A., Siero, J.C.W., Fisher, J.A., Froeling, M., Luijten, P., Philippens, M., Hoogduin, H., 2014. Investigating the non-linearity of the BOLD cerebrovascular reactivity response to targeted hypo/hypercapnia at 7T. *Neuroimage* 98, 296–305. <http://dx.doi.org/10.1016/j.neuroimage.2014.05.006>.
- Blockley, N.P., Driver, I.D., Francis, S.T., Fisher, J.A., Gowland, P.A., 2010. An improved method for acquiring cerebrovascular reactivity maps. *Magn. Reson. Med.* 65, 1278–1286. <http://dx.doi.org/10.1002/mrm.22719>.
- da Costa, L., Fierstra, J., Fisher, J.A., Mikulis, D.J., Han, J.S., Tymianski, M., 2013. BOLD MRI and early impairment of cerebrovascular reserve after aneurysmal subarachnoid hemorrhage. *J. Magn. Reson. Imaging* 40, 972–979. <http://dx.doi.org/10.1002/jmri.24474>.
- Driver, I.D., Andoh, J., Blockley, N.P., Francis, S.T., Gowland, P.A., Paus, T., 2015. Hemispheric asymmetry in cerebrovascular reactivity of the human primary motor cortex: an in vivo study at 7 T. *NMR Biomed.* 28, 538–545. <http://dx.doi.org/10.1002/nbm.3282>.
- Duffin, J., Sobczyk, O., Crawley, A.P., Poulblanc, J., Mikulis, D.J., Fisher, J.A., 2015. The dynamics of cerebrovascular reactivity shown with transfer function analysis. *Neuroimage* 114, 207–216. <http://dx.doi.org/10.1016/j.neuroimage.2015.04.029>.
- Gauthier, C.J., Madjar, C., Desjardins-Crépeau, L., Bellec, P., Bherer, L., Hoge, R.D., 2013. Age dependence of hemodynamic response characteristics in human functional magnetic resonance imaging. *Neurobiol. Aging* 34, 1469–1485. <http://dx.doi.org/10.1016/j.neurobiolaging.2012.11.002>.
- Greve, D.N., Fischl, B., 2009. Accurate and robust brain image alignment using boundary-based registration. *Neuroimage* 48, 63–72. <http://dx.doi.org/10.1016/j.neuroimage.2009.06.060>.
- Jenkinson, M., Bannister, P., Brady, M., Smith, S., 2002. Improved optimization for the robust and accurate linear registration and motion correction of brain images. *Neuroimage* 17, 825–841.
- Jenkinson, M., Beckmann, C.F., Behrens, T.E.J., Woolrich, M.W., Smith, S.M., 2012. FSL. *Neuroimage* 62, 782–790. <http://dx.doi.org/10.1016/j.neuroimage.2011.09.015>.
- Liu, P., Welch, B.G., Li, Y., Gu, H., King, D., Yang, Y., Pinho, M., Lu, H., 2016. Multiparametric imaging of brain hemodynamics and function using gas-inhalation MRI. *Neuroimage*. <http://dx.doi.org/10.1016/j.neuroimage.2016.09.063>.
- Mandell, D.M., Han, J.S., Poulblanc, J., Crawley, A.P., Stainsby, J.A., Fisher, J.A., Mikulis, D.J., 2008. Mapping cerebrovascular reactivity using blood oxygen level-dependent MRI in patients with arterial steno-occlusive disease: comparison with arterial spin labeling MRI. *Stroke* 39, 2021–2028. <http://dx.doi.org/10.1161/STROKEAHA.107.506709>.
- Mazziotta, J., Toga, A., Evans, A., Fox, P., Lancaster, J., Zilles, K., Woods, R., Paus, T., Simpson, G., Pike, B., Holmes, C., Collins, L., Thompson, P., MacDonald, D., Iacoboni, M., Schormann, T., Amunts, K., Palomero-Gallagher, N., Geyer, S., Parsons, L., Narr, K., Kabani, N., Le Goualher, G., Boomsma, D., Cannon, T., Kawashima, R., Mazoyer, B., 2001. A probabilistic atlas and reference system for the human brain: International Consortium for Brain Mapping (ICBM). *Philos. Trans. R. Soc. Lond., B, Biol. Sci.* 356, 1293–1322. <http://dx.doi.org/10.1098/rstb.2001.0915>.
- Mugler, J.P., Brookeman, J.R., 1990. Three-dimensional magnetization-prepared rapid gradient-echo imaging (3D MP RAGE). *Magn. Reson. Med.* 15, 152–157.
- Murphy, K., Bodurka, J., Bandettini, P.A., 2007. How long to scan? The relationship between fMRI temporal signal to noise ratio and necessary scan duration. *Neuroimage* 34, 565–574. <http://dx.doi.org/10.1016/j.neuroimage.2006.09.032>.
- Poulblanc, J., Crawley, A.P., Sobczyk, O., Montandon, G., Sam, K., Mandell, D.M., Duffin, P., Venkatraghavan, L., Duffin, J., Mikulis, D.J., Fisher, J.A., 2015. Measuring cerebrovascular reactivity: the dynamic response to a step hypercapnic stimulus. *J. Cereb. Blood Flow Metab.* 1–11. <http://dx.doi.org/10.1038/jcbfm.2015.114>.
- Poulblanc, J., Han, J.S., Mandell, D.M., Conklin, J., Stainsby, J.A., Fisher, J.A., Mikulis, D.J., Crawley, A.P., 2013. Vascular steal explains early paradoxical blood oxygen level-dependent cerebrovascular response in brain regions with delayed arterial transit times. *Cerebrovasc. Dis. Extra* 3, 55–64. <http://dx.doi.org/10.1159/000348841>.
- Press, W.H., 2007. *Numerical Recipes 3rd Edition*. Cambridge University Press.
- Rodan, L.H., Poulblanc, J., Fisher, J.A., Sobczyk, O., Wong, T., Hlasny, E., Mikulis, D., Tein, I., 2015. Cerebral hyperperfusion and decreased cerebrovascular reactivity correlate with neurologic disease severity in MELAS. *MITOCH* 22, 66–74. <http://dx.doi.org/10.1016/j.mito.2015.03.002>.
- Rostrup, E., Larsson, H.B., Toft, P.B., Garde, K., Thomsen, C., Ring, P., Søndergaard, L., Henriksen, O., 1994. Functional MRI of CO₂ induced increase in cerebral perfusion. *NMR Biomed.* 7, 29–34.
- Sam, K., Small, E., Poulblanc, J., Han, J.S., Mandell, D.M., Fisher, J.A., Crawley, A.P., Mikulis, D.J., 2014. Reduced contralateral cerebrovascular reserve in patients with unilateral steno-occlusive disease. *Cerebrovasc. Dis.* 38, 94–100. <http://dx.doi.org/10.1159/000362084>.
- Slessarev, M., Han, J., Mardimae, A., Prisman, E., Preiss, D., Volgyesi, G., Ansel, C., Duffin, J., Fisher, J.A., 2007. Prospective targeting and control of end-tidal CO₂ and O₂ concentrations. *J. Physiol.* 581, 1207–1219. <http://dx.doi.org/10.1113/jphysiol.2007.129395>.
- Smith, S.M., 2002. Fast robust automated brain extraction. *Hum. Brain Mapp.* 17, 143–155. <http://dx.doi.org/10.1002/hbm.10062>.
- Smith, S.M., Brady, J.M., 1997. SUSAN—a new approach to Low level image processing. *Int. J. Comput. Vis.* 23, 45–78. <http://dx.doi.org/10.1023/A:1007963824710>.
- Sobczyk, O., Battisti-Charbonney, A., Poulblanc, J., Crawley, A.P., Sam, K., Fierstra, J., Mandell, D.M., Mikulis, D.J., Duffin, J., Fisher, J.A., 2015. Assessing cerebrovascular reactivity abnormality by comparison to a reference atlas. *J. Cereb. Blood Flow. Metab.* 35, 213–220. <http://dx.doi.org/10.1038/jcbfm.2014.184>.
- Spano, V.R., Mandell, D.M., Poulblanc, J., Sam, K., Battisti-Charbonney, A., Pucci, O., Han, J.S., Crawley, A.P., Fisher, J.A., Mikulis, D.J., 2012. CO₂ blood oxygen level-dependent MR mapping of cerebrovascular reserve in a clinical population: safety, tolerability, and technical feasibility. *Radiology* 266, 592–598. <http://dx.doi.org/10.1148/radiol.12112795>.
- Suri, S., Mackay, C.E., Kelly, M.E., Germuska, M., Tunbridge, E.M., Frisoni, G.B., Matthews, P.M., Ebmeier, K.P., Bulte, D.P., Filippini, N., 2015. Reduced cerebrovascular reactivity in young adults carrying the APOE ε4 allele. *Alzheimer's Dementia* 11. <http://dx.doi.org/10.1016/j.jalz.2014.05.1755>, 648–657.e1.
- Van Dijk, K.R.A., Sabuncu, M.R., Buckner, R.L., 2012. The influence of head motion on intrinsic functional connectivity MRI. *Neuroimage* 59, 431–438. <http://dx.doi.org/10.1016/j.neuroimage.2011.07.044>.
- Woolrich, M.W., Jbabdi, S., Patenaude, B., Chappell, M., Makni, S., Behrens, T., Beckmann, C., Jenkinson, M., Smith, S.M., 2009. Bayesian analysis of neuroimaging data in FSL. *Neuroimage* 45, S173–S186. <http://dx.doi.org/10.1016/j.neuroimage.2008.10.055>.
- Zhang, Y., Brady, M., Smith, S., 2001. Segmentation of brain MR images through a hidden Markov random field model and the expectation-maximization algorithm. *IEEE Trans. Med. Imaging* 20, 45–57. <http://dx.doi.org/10.1109/42.906424>.